Journal of Magnetics 10(1), 14-22 (2005)

The Presence and Role of Intergranular Phase in $Nd_8Fe_{86-x}Nb_xB_6$ (x = 0, 1, 2, 3) Nanocomposite Magnet Characterized by Mössbauer Spectroscopy

Jong Soo Han[1], Choong Jin Yang*, Eon Byeung Park and Eng Chan Kim[1]

Nanotechnology Research Lab., Research Institute of Industrial Science & Technology (RIST), Pohang City, 790-330, P. O. Box 135, Korea
[1]Department of Physics, Yeungnam University, Gyungsan City 712-749, Korea

(Received 22 February 2005)

Precisely refined Mössbauer study and nano structure observation revealed that intergranular phase formed between α-Fe and $Nd_2Fe_{14}B$ phase in NdFeNbB alloys plays a significant role on the magnetic properties. The intergranular interaction was characterized in term of Henkel Plot (δM plot), and hyperfine field, quardrupole splitting and isomer shift were refined to predict the presence and role of the intergranular phase. By the addition of Nb into $Nd_8Fe_{86}B_6$ composition, coercivity was found to increase by 25% due to the refinement of average grain size of both the soft and hard magnetic phases which was decreased from 50 nm of virgin $Nd_8Fe_{86}B_6$ to 25 nm in $Nd_8Fe_{85}Nb_1B_6$ alloys. The role of Nb addition was confirmed to stabilize the $Nd_2Fe_{14}B$ lattice preventing from thermal vibration of the corresponding sites substituted Fe by Nb atoms in all sites in the $Nd_2Fe_{14}B$ lattice. The enhanced coercivity was originated from the exchange hardening of soft and amorphous phases surrounding the hard magnetic $Nd_2Fe_{14}B$ crystal.

Key words : nanocomposite, Mössbauer, exchange interaction

1. Introduction

Since the nanocomposite magnet has been introduced aiming for its high performance, low cost and extensive applications, the representative compositions such as $Nd_2Fe_{14}B$+Fe_3B [1], $Nd_2Fe_{14}B$+(α-Fe) [2] and $Sm_2Fe_{17}N_x$ +(α-Fe) [3] were studied extensively. Theoretically nanocomposite magnetic materials are well known that their enhanced magnetic properties are attributed to an exchange interaction taking place across the neighboring soft and hard magnetic phases. Therefore the exchange interaction is sensitively depend upon the microstructure such as size, shape, distribution and volume fraction of each magnetically soft and hard phase grains [4, 5]. The most striking feature of those nanocomposites is that typical computer simulation reported some nanocomposite structure could possibly exhibit the maximum energy product values much higher than those obtained from the present experimental achievements. For instance, the simulations reported the energy product values of 800 kJ/m^3 (100 MGOe) from $Sm_2Fe_{17}N_x$+(α-Fe) nanocomposites [4], 400 kJ/m^3 (50 MGOe) from $Nd_2Fe_{14}B$+(α-Fe) nanocomposite [5, 6] structures. Accordingly most of the experimental works focused on the exchange coupling interactions taking place between neighboring magnetic crystalline grains for achieving the highest magnetic properties including the present authors [13, 20].

According to micromagnetic simulations, the highest maximum energy product could be obtained from intergranular phase or phases having suitably small exchange constant for reducing the intergranular interaction between soft and hard phases [6, 7]. However, we found that the residual existence of the amorphous phase leading to the formation of the nano phase mixture plays an important role in the appearance of the hard magnetic properties with the rather high energy products. The superior remanence and coercivity values of those nanocomposite magnets inevitably occur as the results of the exchange coupling between intergranular ferromagnetic phases [8, 9]. It is suggested therefore that a precise investigation on the nature of the intergranular phases is necessary by one way or other in the course of aiming for the most superior magnetic properties [13, 20].

In the present study the authors handled the nanocomposite magnetic ribbons of virgin $Nd_8Fe_{86}B_6$ alloy,

*Corresponding author: Tel: +82-54-279-6331,
e-mail: cjyang@rist.re.kr

and controlled the nano structures by adding Nb from zero to 3 atomic percent enriching the intergranular phase formed between $Nd_2Fe_{14}B$ and Fe grains. The type and force of exchange interaction were characterized by plotting Henkel formulation (δM) [10]. The investigation of the magnetic performance occurring at intergranular phases was analyzed basically by Mössbauer spectroscopy performed at the temperature range of 100~300 K. Subsequently, we focused the effect of Nb on the enhanced magnetic properties and intergranular interaction, and identified the nature of nanocomposite structure according to the observed magnetic behaviors.

2. Experiment

Ingots of $Nd_8Fe_{86-x}Nb_xB_6$ (x = 0, 1, 2, 3) composition were prepared homogeneously by plasma arc melting under Ar atmosphere. The sample powders were prepared by extractive plasma arc melt spinning employing a wheel speed during spinning of 20 m/sec [19]. The amorphous melt spun ribbon precursors were annealed for 10 min at vacuum atmosphere of 10^{-6} Torr range at the temperature ranges of 590~770 °C. All the magnetic properties were measured using a vibrating sample magnetometer. Exchange coupling behaviors were finely analyzed using a very sensitive alternative gradient magnetometer having a measuring sensitivity of 10^{-9} emu for those nano scale materials. Coupling interactions could be demonstrated in detail by the Henkel plots (δM plot). Crystallization of the amorphous ribbons was confirmed by x-ray diffractometry and filed emission transmission electron microscopy. Mössbauer spectra of $Nd_8Fe_{86}B_6$ and $Nd_8Fe_{86-x}Nb_xB_6$ (x = 0, 1, 2, 3) were taken at the temperatures 100, 150, 200, 250 and 300 K with a transmission electron Mössbauer spectroscopy (TEMS). The spectra were evaluated by using a model of distribution of hyperfine field and seven sextet of Lorentzian lines employing the PCMOS II program [13].

3. Results and Discussion

3.1. Microstructure and Magnetic Properties

All the nanocomposite precursors were amorphous after rapid solidification in this study, and the maximum properties were obtained by following an optimized heat treatment for each amorphous melt spun ribbons. Therefore, the relationship from the initial amorphous state to the final magnetic properties was characterized via x-ray diffractometry, field emission transmission electron microscopy.

Fig. 1 shows the magnetic properties measured from

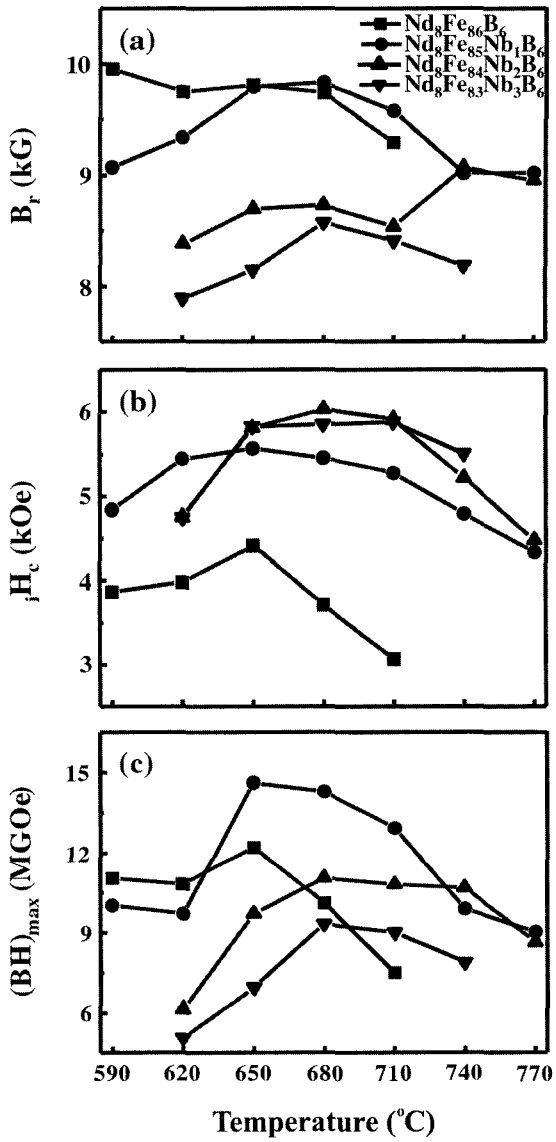

Fig. 1. Magnetic properties as a function of annealing temperature.

melt spun ribbons followed by optimized annealing. The maximum values which were obtained from $Nd_8Fe_{85}Nb_1B_6$ composition annealed at 650 °C for 10 min were: B_r = 9.791 kG, $_iH_c$ = 5.565 kOe and $(BH)_{max}$ = 14.61 MGOe. The coercivity values were confirmed to increase by the addition of paramagnetic element Nb from 1 to 3 at.%, but rather the remanence values were found to decrease in the order of addition of Nb in general. As can be seen in Fig. 1, the optimized properties are obtained from the nanocomopsite of NdFeNbB containing the Nb of 1 at.%. From this result the study was focused on a comparison between $Nd_8Fe_{86}B_6$ and $Nd_8Fe_{85}Nb_1B_6$ for investigating the effect of Nb. The remarkably enhanced property is shown in Fig. 1(b) where the coercivity value is very

much increased by the addition of 1 at.% Nb into the virgin $Nd_8Fe_{86}B_6$ composition. Basically both the coercivity and remanence values for virgin $Nd_8Fe_{86}B_6$ tend to decrease as a function of annealing temperature, however, the $Nd_8Fe_{85}Nb_1B_6$ nanocomposite shows the maximum properties after the treatment at 650 °C, and then decreases thereafter. Therefore the addition of Nb below 1~3 at.% is believed to have the effect of grain refinement [8, 9]. This looks very reasonable by considering the higher melting point of Nb(T_m = 2740 °C) compared with those of Fe (T_m = 1809 °C) and Nd (T_m = 1289 °C). The access addition of Nb, however, would be harmful due to the paramagnetic character of Nb atoms which is proven by the deteriorated remanence values shown in all the figures (a), (b) and (c).

Fig. 2 and 3 show x-ray diffraction patterns and TEM photographs for the as-spun and annealed samples, respectively. In general, the crystallization behaviors from amorphous materials of both the virgin $Nd_8Fe_{86}B_6$ and

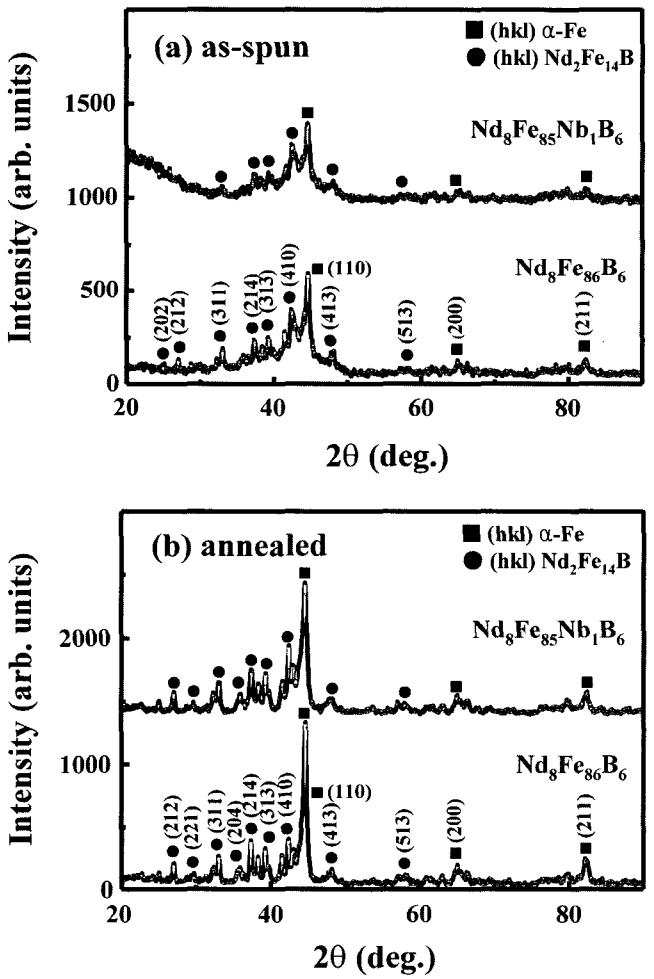

Fig. 2. X-ray diffraction patterns of ribbons (a) as-spun and (b) annealed at 650°C/10 min.

$Nd_8Fe_{85}Nb_1B_6$ seem to have identical transformation after spinning as shown in Fig. 2(a), even after the annealing treatment as shown in Fig. 2(b). Only the difference is that even after the spinning the x-ray pattern indicates the formation of very fine crystallites for both the alloys. Therefore it is necessary to take a close look at their microstructure using a high resolution transmission electron microscope. Fig. 3 shows more detailed nanostructures of amorphous and nanocrystalline distribution which was not possible via x-ray diffractometry. In the amorphous matrix of the virgin $Nd_8Fe_{86}B_6$ alloy, short-range ordered crystallite embryos start to form already ranging over the size of 50 nm as shown in Fig. 3(a). However, the same crystallites can not be seen in the as- spun $Nd_8Fe_{85}Nb_1B_6$ matrix in Fig. 3(b) but only amorphous like particles are formed which is not clearly resolvable even by the field emission electron microscope. Accordingly this trend tend to keep after the heat treatment resulting in nanocrystals having the grain size less than 25 nm as shown in Fig. 3(d). These nano crystals basically enhanced the coercive force.

When the addition of Nb is excessive more than 1 at.%, the problem is that the coercivity increases at the expense of remanence values. Since the remanence and coercivity at the annealing temperature of 650 °C for both the $Nd_8Fe_{85}Nb_1B_6$ and $Nd_8Fe_{86}B_6$ are the same as shown in Fig. 1, the authors infer that the effect of intergranular exchange interaction would be similar each other. Subsequently detailed analysis of the exchange coupling behavior was investigated and the results are shown in the Henkel plot in Fig. 4. Using the alternative gradient magnetometer the authors measured isothermal AC remanence curves, $I_r(H)$, and DC demagnetization curves, $I_d(H)$ of concerned nanocomposite samples. The degree of exchange coupling can be examined by plotting $dM(H)$ curves which is eventually possible by defining Wohlfarth's single domain particle model again as follows [21]:

$$I_d(H) = I_r(\infty) - 2\, I_r(H)$$

The relationship was proposed for particles in the range of single domain without any interaction between them. Later Kelly et al. extended the relationship to exchange coupled particles such as nanocomposite materials using the residual moment and coercivity difference as well measured from $I_r(H)$ and $I_d(H)$ curves:

$$I_d(H)/I_r(\infty) = 1-2\, I_r(H)/I_r(\infty) + \delta M(H)$$

$\delta M(H)$ curves for both the $Nd_8Fe_{85}Nb_1B_6$ and $Nd_8Fe_{86}B_6$ are plotted in Fig. 4. The negative $\delta M(H)$ values which is plotted below zero for $Nd_8Fe_{86}B_6$ alloy only shows that the magetostatic interaction is the major reaction between

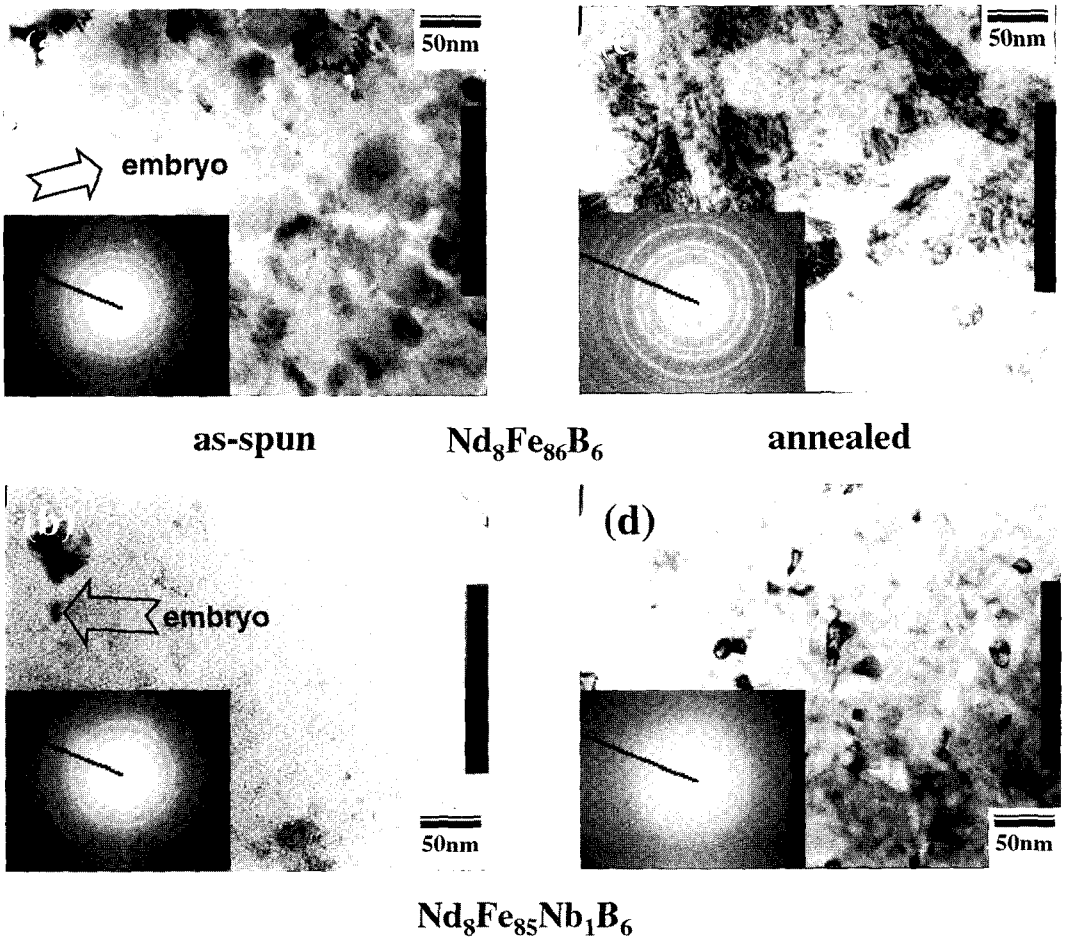

Fig. 3. Microstructure and electron diffraction patterns of ribbons (a), (b) as-spun (left) and (c) (d) annealed (right) at 650 °C/10 min.

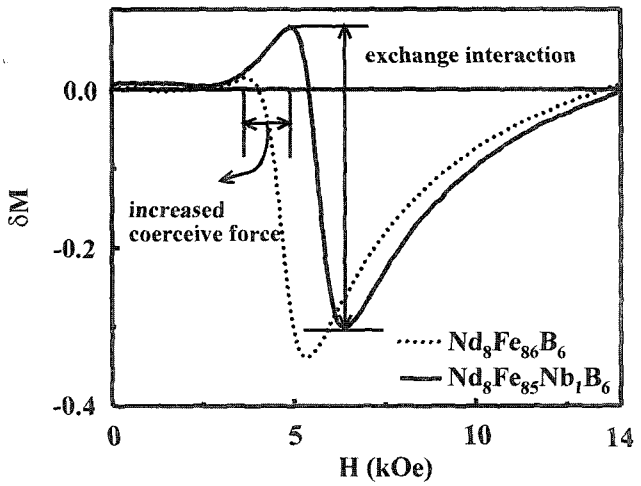

Fig. 4. Henkel plot of $Nd_8Fe_{86}B_6$ and $Nd_8Fe_{85}Nb_1B_6$ annealed at 650 °C for 10 min.

magnetically hard and soft grains. However, the $\delta M(H)$ values transited from positive to negative values for $Nd_8Fe_{85}Nb_1B_6$ nanocomopsite indicate active interactions between the nanocrystals of magnetic phases. The increased coercive value difference about 2.5 kOe indicated by the positive peaks along the $\delta M(H)$curves of two different compositions means that the nucleation magnetic field for reversing the magnetic domain for $Nd_8Fe_{85}Nb_1B_6$ nanocomposite is hard to be reversed due to the spring back force originated by coupling interaction.

3.2. Mössbauer spetra analysis of the presence of amorphous phase

Mössbauer spectra of both the $Nd_8Fe_{86}B_6$ and $Nd_8Fe_{85}Nb_1B_6$ looks very complicated having one nonequivalent site of α-Fe, six of $Nd_2Fe_{14}B$ and amorphous phase. Therefore we are constrained to assume for obvious analysis as follows: (a) Mössbauer spectra containing amorphous phases are very similar and consist of structureless absorption lines that are broadened by distribution of magnetic hyperfine field, quadrupole splitting and isomer shifts. Those broadened lines may be analyzed in terms of

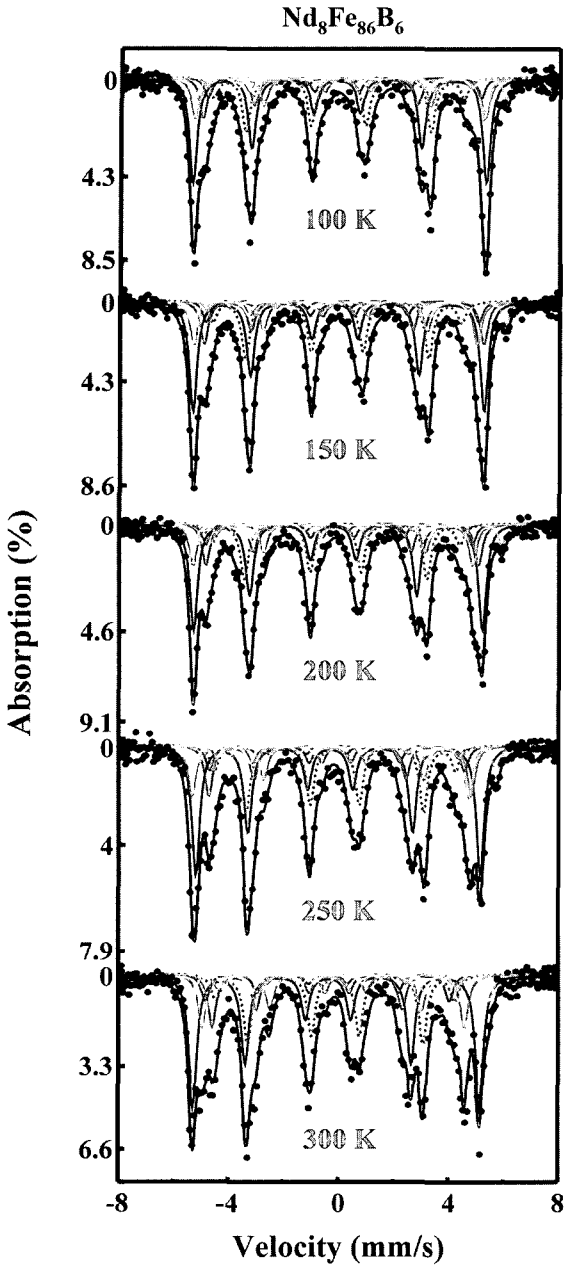

Fig. 5. Mössbauer spectra of $Nd_8Fe_{86}B_6$ and refined curves at the denoted temperature. The hyperfine field distribution (HFD) is represented by a dashed line.

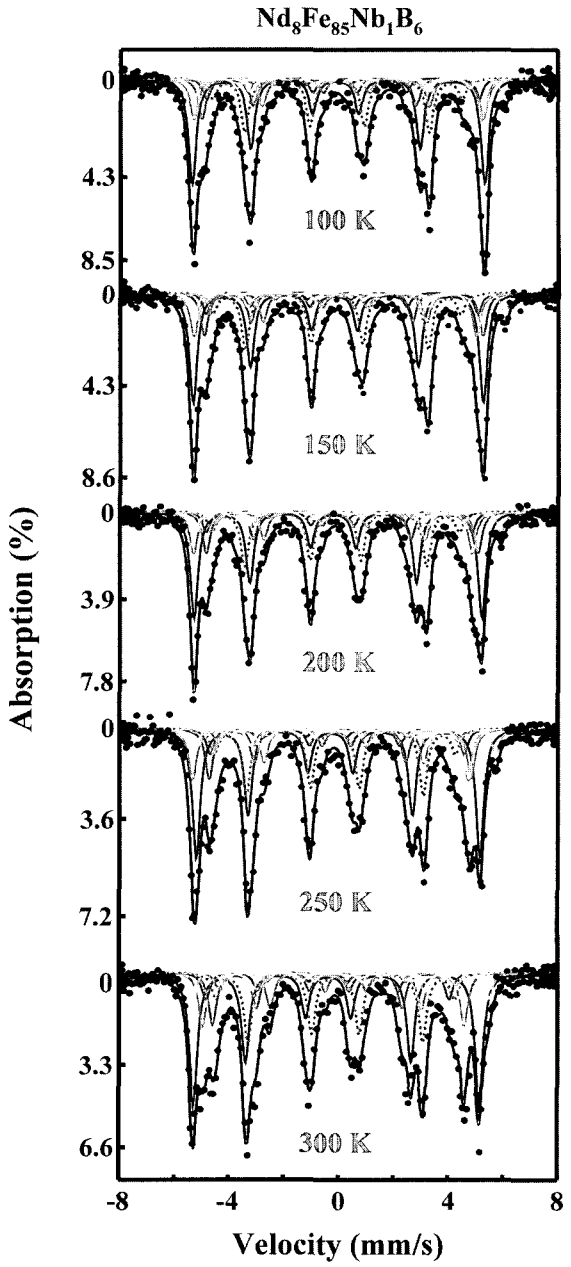

Fig. 6. Mössbauer spectra and refined curves of $Nd_8Fe_{85}Nb_1B_6$ at the denoted temperature. The hyperfine field distribution (HFD) is represented by a dashed line.

distribution of magnetic hyperfine field assuming that broadening from distributions of quadrupole splitting and isomer shift are insignificant in this work [10]. (b) The line width and intensity ratio of α-Fe and $Nd_2Fe_{14}B$ are assumed to be identical at all temperatures because the temperature dependence of the recoilless fractions of Fe atoms at the different sites assumed to be the same [11-14]. (c) The area ratios for k_1, k_2, j_1, j_2, e, and c sites of $Nd_2Fe_{14}B$ are constrained to be 4:4:2:2:1:1 because those sites have Fe atoms of 16, 16, 8, 8, 4, and 4, respectively, for the same recoilless fractions [11-14]. Mössbauer spectra of $Nd_8Fe_{86}B_6$ and $Nd_8Fe_{85}Nb_1B_6$ obtained between 100 and 300 K are fitted in Fig. 5 and 6. Mössbauer spectra for these alloys are commonly decomposed into six nonequivalent site of $Nd_2Fe_{14}B$, one of α-Fe and one of amorphous. The subspectrum with hyperfine field distribution caused by amorphous is represented by the dashed line in Fig. 5 and 6. The distribution of amorphous phases are not randomly localized but rather uniformly distributed embryos are seen as in the Fig. 3, which may be ideal

Table 1. Mössbauer parameters, hyperfine field (HF), isomer shift (IS) and quadrupole splitting (QS) obtained at room temperature

Alloy	Phase	Site	HF (T)	IS (mm/s)	QS (mm/s)	Volume (%)
$Nd_8Fe_{86}B_6$	α-Fe		32.36	–0.21	0.3	33.8
	$Nd_2Fe_{14}B$	$16k_1$	28.49	–0.15	0.33	13.2
		$16k_2$	29.60	0.06	–0.46	13.4
		$8j_1$	27.54	–0.38	–0.01	6.6
		$8j_2$	33.66	0.4	0.06	6.6
		4e	24.26	0.36	–1.20	3.3
		4c	27.07	–0.04	0.02	3.3
	intergranular			–0.03	–0.13	19.8
$Nd_8Fe_{85}Nb_1B_6$	α-Fe		31.54	–0.15	0.45	24.2
	$Nd_2Fe_{14}B$	$16k_1$	28.71	–0.13	0.39	16.4
		$16k_2$	30.63	–0.05	–0.67	16.3
		$8j_1$	26.67	–0.43	0.17	6.8
		$8j_2$	33.80	–0.18	0.64	6.8
		4e	23.20	0.08	–0.37	3.4
		4c	26.38	0.09	0.00	3.4
	intergranular			0.17	–0.64	22.7

for the high performance nanocomposite magnets [15].

It is well utilized that the relative intensities of Mössbauer absorption lines give clues of information about the magnetic moments. The relative intensity ratio of the second to the first or the fifth to the sixth lines, $A_{2,5}/A_{1,6}$, is given by $A_{2,5}/A_{1,6} = 4\sin^2\theta/3(1+\cos^2\theta)$ where θ is the angle between γ-ray and the direction of the magnetic hyperfine field [10]. The ratio $A_{2,5}/A_{1,6}$ is confirmed to vary from 0 to 4/3 as θ changes from 0 to 90°. In the present study Mössbauer spectra were collected with the γ-ray bombarding perpendicular to the plane of ribbon samples. The relative intensity ratio from crystalline phases in the present study was assumed to have 3:2:1:1:2:3 of the Zeeman line since the sample consists of multicrystals. And then we can obtain the best fit for the amorphous phase at $\theta = 0.0293°$. This means that the amorphous phase has an almost perpendicular anisotropy like $Fe_{82}B_{12}Si_6$(METGLAS) produced by melt-spinning [16]. The parameters of each subspectra measured at room temperature are summarized in Table 1. The volume fraction of α-Fe decreases rather those of $Nd_2Fe_{14}B$ and intergranular phases tend to increase by adding Nb. This sounds reasonable taking into account the previous result that Nb become enriched in the amorphous regions during crystallization process [8, 9]. Nevertheless adding the paramagnetic Nb element results in enhanced exchange interaction which again makes the remanence values of $Nd_8Fe_{86}B_6$ and $Nd_8Fe_{85}Nb_1B_6$ be almost the same as in the Fig. 1. It is noteworthy, therefore, that improving the exchange interaction between the crystalline grains can be controlled not only by the volume fraction of hard and soft magnetic crystals but also by the volume fraction of residual amorphous phase and structure as well as was suggested in the previous studies [8, 9].

It is well known that for crystalline ferromagnets, the magnetization M(T) at low temperatures decreases as a function of $T^{3/2}$, Bloch's law. From this the following equation is suggested as [12]:

$$q(T)=q(0)(1-BT^{3/2})$$

where B is a coefficient related to Debye temperature, and $q(=eV_{zz})$ is the principal axis of the electric field gradient (EFG) having the V_{zz} neighboring atoms in z direction, in this case, c axis of $Nd_2Fe_{14}B$ crystal. This dependence has its origin mainly in the thermal vibration of the $Nd_2Fe_{14}B$ lattices. It is known that the quadrupole splitting (Δ) is related to the angle θ between the direction of the hyperfine field and the principal axis of the EFG by the equation [12]:

$$\Delta=\frac{1}{4}eqQ(3\cos^2\theta-1)\left[1+\frac{\eta^2}{3}\right]^{1/2}$$

where Q is the nuclear quadruple moment and η is the asymmetry parameter. The change of angle θ will lead to an abrupt change in the quadrupole splitting. The source is of course a spin reorientation. Fig. 7 and 8 show temperature dependence of quadrupole splitting and isomer shift for $Nd_8Fe_{86}B_6$ and $Nd_8Fe_{85}Nb_1B_6$ lattices, respectively. Basically the addition of Nb having a very high melting temperature tends to prevent from vibrating the overall atomic lattices including 4c site. Actually 4c site

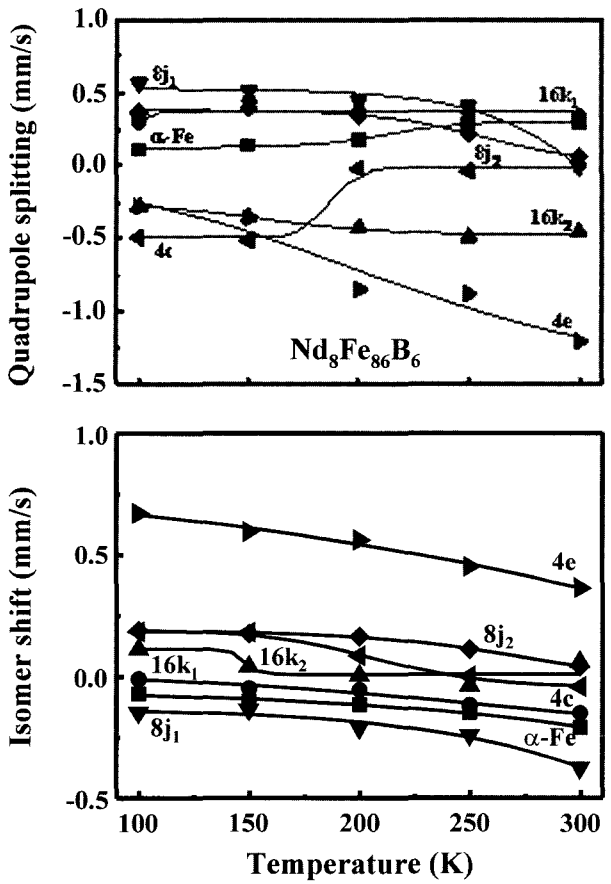

Fig. 7. Temperature dependence of quadrupole splitting, and isomer shift for $Nd_8Fe_{86}B_6$.

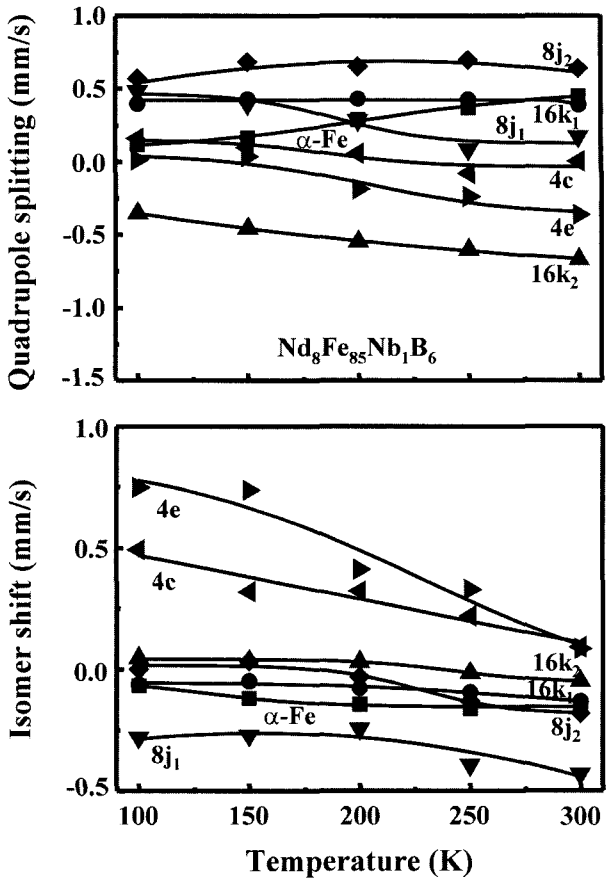

Fig. 8. Temperature dependence of quadrupole splitting, and isomer shift for $Nd_8Fe_{85}Nb_1B_6$.

is surrounded by the largest neighboring atoms of Nd and the lowest of Fe, and indicates an abrupt change above 180 K in $Nd_8Fe_{86}B_6$ especially in Fig. 7(a) and (b). However, after adding Nb atoms into $Nd_2Fe_{14}B$ lattice the temperature dependences of the almost every sites agree well with the linear relationship as shown in Fig 8(a) and (b). This means that Nb atoms have lots of chances to be clustered with or substituted with Fe at c site too which is not possible in the virgin NdFeB alloys. For instance $Nd_8Fe_{85}Nb_1B_6$ containing 1 at.% Nb does not show any abrupt change in the both quadrupole splitting and isomer shift along with the temperature rise in Fig. 8(a) and (b) but shows ordinary behaviors. However more detailed and advanced analysis is demanded by a further research.

The temperature dependence can be most clearly seen by plotting the change of hyperfine field as a function of $T^{3/2}$, as shown in Fig. 9 for alloys $Nd_8Fe_{86}B_6$ and $Nd_8Fe_{85}Nb_1B_6$. The temperature coefficient (B) of hyperfine field is given by the formula [17, 18]:

$$B=\frac{1}{T^{3/2}}\left[1-\frac{H_{hf}(300K)}{H_{hf}(0K)}\right]$$

H_{hf}(0 K) was calculated with the least-squares method, and the calculated B values using measured H_{hf}(300 K) are tabulated in Table 2. B increases in inversely proportion to ferromagnetic exchange interaction indicating a deterioration of the exchange interaction. The exchange interaction of $16k_1$, $16k_2$ and $8j_1$ sites increase rather those of $8j_2$, 4e and 4c sites decrease in $Nd_2Fe_{14}B$ lattice. Especially the exchange interaction of α-Fe seems to decrease almost double by adding Nb. This may rationalize that the improved coercivity in $Nd_8Fe_{85}Nb_1B_6$ alloys is mainly caused by the well distributed amorphous interface boundary in the nanocomposite structure which induce the enhanced exchange hardening [5] not by the enhanced hyperfine filed of $Nd_2Fe_{14}B$ lattice. As shown in Fig. 10, the temperature dependence of intergranular phase looks more linear for $Nd_8Fe_{85}Nb_1B_6$ alloy than $Nd_8Fe_{86}B_6$. We assure that the linearity of $T^{3/2}$ law may be significant on the thermal stability of the magnetic phase, which is well confirmed by the addition of Nb atoms. However, the addition of Nb atoms into appropriate atomic sites of $Nd_2Fe_{14}B$ lattice seems to stabilize the lattice in terms of quadrupole splitting and isomer shift.

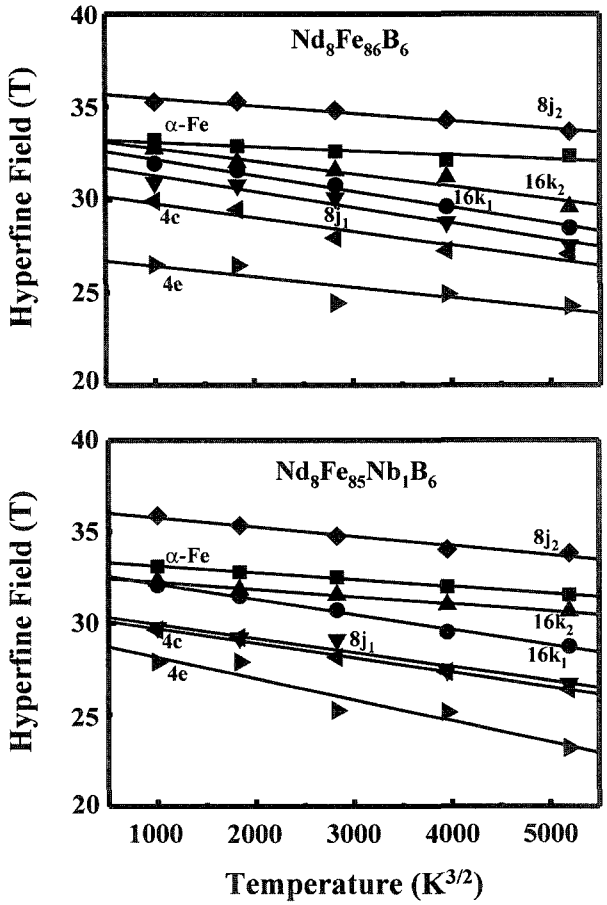

Fig. 9. Temperature dependence of hyperfine field for $Nd_8Fe_{86}B_6$ and $Nd_8Fe_{85}Nb_1B_6$.

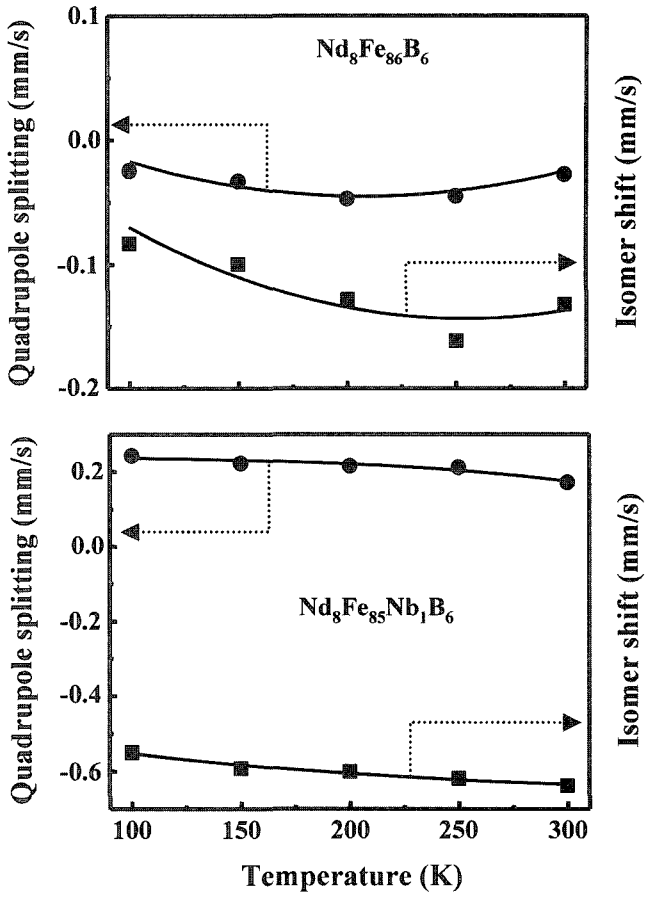

Fig. 10. Temperature dependence of quadrupole splitting, and isomer shift of intergranular phase.

4. Conclusion

It is very important to make amorphous precursor materials having well distributed and fine enough embryos to have high performance nanocomposite magnets in FeNdB system containing high melting temperature transition element. The added high melting temperature elements will substitute with Fe atoms at a certain sites preferably in the $Nd_2Fe_{14}B$ lattice. The present study shows that 4c site is a typical site where Nb atoms is clustered with Fe preferably. The addition of an appropriate transition element tends to stabilize the $Nd_2Fe_{14}B$ lattice and prevent from thermal vibration which eventually induces enhanced magnetic properties in terms of hyperfine field, quadrupole splitting and isomer shift. The addition of Nb into NdFeB system enhances coercivity values by adjusting an appropriate nano structures in the nanocomposite of $Nd_2Fe_{14}B$+Fe+amorphous composite magnets, especially by well distributed amorphous intergranular material, not by the increase of hyperfine filed of the $Nd_2Fe_{14}B$ lattice. The intergranular amorphous phase in nanocomposite magnet was confirmed to have a perpendicular anisotropy like in the Fe based METGLAS.

Acknowledgement

The support by MOCIE (Dual Use Technology Project) under project No. 2004D025 is gratefully acknowledged.

Table 2. Temperature coefficients of H_{hf} for the six and one nonequivalent sites in $Nd_2Fe_{14}B$ and α-Fe, respectively

	B ($\times 10^{-5}$)						
Site	α-Fe	$16k_1$	$16k_2$	$8j_1$	$8j_2$	4e	4c
$Nd_8Fe_{86}B_6$	0.5486	2.6354	2.211	2.7529	1.1838	1.9416	2.1804
$Nd_8Fe_{85}Nb_1B_6$	1.11	2.4665	1.1681	2.5092	1.3042	3.9829	2.588

References

[1] R. Coehoorn, D. B. de Mooij, and C. de Waard, J. Magn. Magn. Mater. **80**, 101 (1989).

[2] A. Manaf, R. A. Buckley, and H. A. Davies, J. Magn. Magn. Mater. **128**, 302 (1993).

[3] J. Ding, P. G. McComick, and R. Street, J. Magn. Magn. Mater. **124**, 1 (1993).

[4] R. Skomski and J. M. D. Coey, Phys. Rev. B **48**, 15812 (1993).

[5] T. Schrefl, R. Fischer, J. Fidler, and H. Kronmüller, J. Appl. Phys. **76**, 7053 (1994).

[6] T. Schrefl, H. Roitner, and J. Fidler, J. Appl. Phys. **81**, 5567 (1997).

[7] H. Fukunaga, J. Kuma, and Y. Kanai, IEEE. Trans. Magn. **35**, 3235 (1999).

[8] T. Kobayashi, M. Yamasaki, and M. Hamano, J. Appl. Phys. **87**, 6579 (2000).

[9] M. Yamasaki, M. Hamano, H. Mizuguchi, T. Kobayashi, K. Hono, H. Yamamoto, and A. Inoue, Scripta. Mater. **44**, 1375 (2001).

[10] H. N. Ok and A. H. Morrish, Phys. Rev. B **22**, 4215 (1980).

[11] R. Kamal and Y. Andersson, Phys. Rev. B **32**, 1756 (1985).

[12] Z. W. Li, X. Z. Zhou, and A. H. Morrish, Phys. Rev. B **41**, 8617 (1990).

[13] C. J. Yang, E. B. Park, J. S. Han, and E. C. Kim, Phys. Stat. Sol. (a) **201**, 1951 (2004).

[14] C.J. Yang, E. B. Park, J. S. Han, and E. C. Kim, J. of Magnetics **9**(2), 27 (2004).

[15] T. J. Konno, M. Uehara, S. Hirosawa, J. Sumiyama, and K. Suzuki, J. Alloys. Compd. **268**, 278 (1998).

[16] H. N. Ok and A. H. Morrish, Phys. Rev. B **23**, 2257 (1981).

[17] B. X. Gu, D. S. Xue, B. G. Shen, and F. S. Li, J. Magn. Magn. Mater. **167**, 150 (1997).

[18] C. L. Chien and R. Hasegawa, Phys. Rev. B **16**, 2114 (1977).

[19] C. J. Yang, E. B. Park, and S. D. Choi, Mater. Lett. **24**, 347 (1995).

[20] C. J. Yang and E. B. Park. J. Magn. Magn. Mater. **168**, 278 (1997).

[21] E. P. Wohlfarth, J. Appl. Phys. **29**, 595 (1958).